A tick salivary protein targets cathepsin G and chymase and inhibits host inflammation and platelet aggregation

Jindrich Chmelar,[1,2] Carlo J. Oliveira,[3] Pavlina Rezacova,[4] Ivo M. B. Francischetti,[5] Zuzana Kovarova,[4] Gunnar Pejler,[6] Peter Kopacek,[1] José M. C. Ribeiro,[5] Michael Mares,[4] Jan Kopecky,[1] and Michail Kotsyfakis[1]

[1]Institute of Parasitology, Biology Centre of the Academy of Sciences of Czech Republic, Ceske Budejovice, Czech Republic; [2]Faculty of Science, University of South Bohemia, Ceske Budejovice, Czech Republic; [3]Department of Biochemistry and Immunology, School of Medicine of Ribeirão Preto, University of São Paulo, Ribeirão Preto, Brazil; [4]Institute of Organic Chemistry and Biochemistry of the Academy of Sciences of Czech Republic, Prague, Czech Republic; [5]National Institute of Allergy and Infectious Diseases, National Institutes of Health, Rockville, MD; and [6]Department of Anatomy, Physiology and Biochemistry, Biomedical Centre, Swedish University of Agricultural Sciences, Uppsala, Sweden

Platelet aggregation and acute inflammation are key processes in vertebrate defense to a skin injury. Recent studies uncovered the mediation of 2 serine proteases, cathepsin G and chymase, in both mechanisms. Working with a mouse model of acute inflammation, we revealed that an exogenous salivary protein of *Ixodes ricinus*, the vector of Lyme disease pathogens in Europe, extensively inhibits edema formation and influx of neutrophils in the inflamed tissue. We named this tick salivary gland secreted effector as *I ricinus* serpin-2 (IRS-2), and we show that it primarily inhibits cathepsin G and chymase, while in higher molar excess, it affects thrombin activity as well. The inhibitory specificity was explained using the crystal structure, determined at a resolution of 1.8 Å. Moreover, we disclosed the ability of IRS-2 to inhibit cathepsin G-induced and thrombin-induced platelet aggregation. For the first time, an ectoparasite protein is shown to exhibit such pharmacological effects and target specificity. The stringent specificity and biological activities of IRS-2 combined with the knowledge of its structure can be the basis for the development of future pharmaceutical applications. (*Blood*. 2011; 117(2):736-744)

Introduction

The first response of a vertebrate organism to a skin injury involves blood coagulation, vasoconstriction, platelet aggregation, and innate immune mechanisms, such as inflammation and complement activation, that have an important antibacterial role. Upon a tick bite, these mechanisms are activated as a first line of defense and are dependent, among others, on serine protease cascades (in blood coagulation and complement activation) or on the proteolytic activation of bioactive peptides, such as chemokines, vasoconstrictors, or protease-activated receptors (PARs). Previous studies demonstrated that these serine protease–dependent processes are regulated by endogenous inhibitors. To prevent pathophysiological conditions, proteases and inhibitors must be in balance; in the case of an exogenous inhibitor (eg, of parasitic origin) infiltrating the system, this balance will be impaired.

This phenomenon is also observed in the saliva of hematophagous arthropod ectoparasites, including ticks.[1] The saliva of ixodid ticks plays a crucial role at the tick-host interface not only because it contains numerous proteins that affect many host nonspecific defensive mechanisms, such as inflammation, blood coagulation, and platelet aggregation, but also because it can target acquired immunity.[2] Activation of these host physiological mechanisms immediately after a tick bite would be detrimental for tick feeding success, and therefore it is vital for the tick to overcome them. Investigation of the underlying mechanism, although time consuming, revealed salivary constituents with pharmacologic activities targeting vertebrate host defense, including molecules with anti-inflammatory potential.[3,4] This process was accelerated by recent transcript-sequencing projects on tick salivary glands (ie, sialotranscriptomics), where numerous salivary protein candidates were identified that may account for the pharmacologic properties of tick saliva.[5-7]

Of interest, a number of genes encoding for potential serine protease inhibitors were identified in *Ixodes spp* salivary glands, including serpins, the largest, most diverse family of protease inhibitors. The mode of action of serpins is unique and depends on their folding and the primary structure of specific conserved domains. The literature dealing with the structural and functional properties of serpins and the evolution of this protein family is reviewed elsewhere.[8,9] More than 60 serpins were identified at the sequence level in ixodid ticks, largely due to the completed *I scapularis* genome[10-14]; however, only 1 tick serpin originating from *I ricinus*, the vector of Lyme disease pathogens in Europe, has been functionally characterized.[14] The serpin was named *I ricinus* immunosuppressant (IRIS), and it targets the serine protease, elastase. Despite not bearing a classical secretion signal, it can affect vertebrate hemostasis apart from vertebrate immunity.[15] Recently, Prevot and colleagues showed the involvement of an exosite domain in the anti-inflammatory activity of IRIS. Surprisingly, unlike its antihemostatic activity, the anti-inflammatory properties of IRIS are independent of its inhibitory nature.[16] Thus, the inhibitory function of IRIS was not directly shown to be responsible for its observed immunomodulatory properties, so the answer—whether salivary serpins can mimic the function of vertebrate regulators and thus immunomodulate the host—

Submitted June 25, 2010; accepted September 29, 2010. Prepublished online as *Blood* First Edition paper, October 12, 2010; DOI 10.1182/blood-2010-06-293241.

The online version of this article contains a data supplement.

The publication costs of this article were defrayed in part by page charge payment. Therefore, and solely to indicate this fact, this article is hereby marked "advertisement" in accordance with 18 USC section 1734.

remained undisclosed. The same is true for the structural basis of IRIS function. Apart from IRIS, no other serpin from *I ricinus* has been described to date.

Here, we present the functional characterization of a novel inhibitory serpin from the saliva of the tick, *I ricinus*, that we named *I ricinus* serpin-2 (IRS-2). It bears a clear secretion signal and inhibits edema formation and neutrophil influx in the inflamed tissues in a mouse model of acute inflammation. The protein targets primarily 2 proinflammatory serine proteases, cathepsin G and mast cell chymase, and, in higher molar excess, thrombin. Because of its inhibitory activity, IRS-2 blocks cathepsin G– and thrombin-induced platelet aggregation, thus playing a dual role during tick feeding, as it can interfere with both inflammation and wound healing. We also determined a high-resolution crystal structure of IRS-2 that provides structural insight into the observed inhibitory specificity. This is the first report of the crystal structure of a serpin isolated from a parasitic organism. Moreover, such a mechanism in which the parasite uses inhibition of cathepsin G and chymase to overcome the host defense system, has not been shown for any blood-feeding arthropod salivary constituent to date.

Methods

Unless otherwise indicated, standard procedures were followed,[17] and experiments were performed at room temperature (25 ± 1°C). All water used was of 18-MΩ quality produced by a MilliQ apparatus (Millipore). If not otherwise stated, all reagents were purchased from Sigma-Aldrich, and all cells were cultured at 37°C under an atmosphere of 5% CO_2. The procedures of gene cloning, sequence analysis, real-time polymerase chain reaction (PCR), protein expression, and biochemical methods are detailed in supplemental Methods (available on the *Blood* Web site; see the Supplemental Materials link at the top of the online article).

Paw edema assay

Female C57BL/6 mice (6-8 weeks old) were used. The mice were purchased from The Jackson Laboratory and maintained in the National Institute of Allergy and Infectious Diseases (NIAID) Animal Care Facility under pathogen-free conditions in temperature-controlled rooms, receiving water and food ad libitum. All treatments were performed in accordance with the National Institutes of Health [NIH]'s *Guide for the Care and Use of Laboratory Animals* , and the animal study protocols were approved by the Division of Intramural Research/NIAID Animal Care and Use Committee. The carrageenan-induced hind-paw inflammation model was used to investigate the potential anti-inflammatory role of IRS-2. Before each injection, the basal footpad thickness of each mouse was recorded using a caliper (Mitutoyo America Corp). Subsequently, 40 μL of carrageenan (2% in saline) was administered by intraplantar injection in each footpad in the absence or presence of different concentrations of lipopolysaccharide-free IRS-2. As a control, each group of mice received the same volume of saline (vehicle) in the presence of IRS-2 only. The same experimental design and concentrations were used for chymostatin, a generic protease inhibitor, and indomethacin, a nonsteroid anti-inflammatory compound. Each effector was coadministered with carrageenan in the mouse footpad. As an index of edema formation, paw thickness (in millimeters) was measured at 4 and 24 hours after injection, and myeloperoxidase (MPO) activity was measured to estimate the potential effect of IRS-2 on neutrophil migration. For details, please see supplemental Methods.

Isolation and cultivation of PCMCs

Animal experiments were performed in accordance with protocols approved by the local ethical committee. Peritoneal cells were obtained from 6-8-week-old C57BL/6 mice by lavage of the peritoneal cavity with ice-cold phosphate-buffered saline (PBS), washed in fresh PBS, and resuspended in growth medium. The growth medium was Dulbecco modified Eagle medium with GlutaMAX (Gibco), 10% of conditioned media from Chinese hamster ovary cells transfected with mouse stem cell factor (a gift from Dr Marc Daeron), 10% fetal calf serum, 1% penicillin-streptomycin (Invitrogen), 1% minimum essential medium with nonessential amino acids (Gibco), and 50μM mercaptoethanol. Nonadherent cells (mainly peritoneal cell–derived mast cells [PCMCs]) were collected and resuspended in fresh medium to a concentration 10^5 cells/mL every third day. After 6 weeks of cultivation, the enriched PCMCs were used for experiments.

Preparation of washed human platelets and platelet aggregation assays

Platelet-rich plasma was obtained by plateletpheresis from medication-free, adult, healthy platelet donors at the Department of Transfusion Medicine/NIH blood bank under the direction of Dr S. Leitmann as described elsewhere.[18] Briefly, after the addition of 0.2 U/mL apyrase, platelet-rich plasma was centrifuged at 1100 × *g* for 15 minutes and washed twice by centrifugation in Tyrode buffer (137mM NaCl, 27mM KCl, 12mM $NaHCO_3$, 0.42mM NaH_2PO_4, 1mM $MgCl_2$, 5.55mM glucose, 0.25% bovine serum albumin; pH 7.4). Platelets were resuspended in apyrase-free Tyrode buffer and adjusted to a concentration of 200 000-400 000 platelets/μL. Washed human platelets (300 μL) were placed in a Chrono-Log Lumi-aggregometer (Chrono-Log Corp) and stirred at 1200 rpm at 37°C for 1 minute, followed by the addition of reagents, as indicated in the figure legends. In all experiments, 1.5μM IRS-2 was preincubated for 15 minutes with the various effectors tested, and the mixture was added to platelets.

Crystallization and data collection

Details of the crystallization procedure and diffraction data collection are reported elsewhere.[19] Crystals of IRS-2 were prepared at 20°C using the hanging-drop, vapor-diffusion technique. The crystallization drop consisted of 2 μL of the IRS-2 solution (3.5 mg/mL in 20mM HEPES [N-2-hydroxyethylpiperazine-N′-2-ethanesulfonic acid]; pH 7.2) and 1 μL of the reservoir solution (75mM MES [2-(N-morpholino)ethanesulfonic acid], pH 6.5, 9% [wt/vol] polyethylene glycol 20 000). For data collection, crystals were soaked in reservoir solution supplemented with 20% (vol/vol) polyethylene glycol 400 and flash-cooled in liquid nitrogen. Diffraction data were collected at 100 K using the X12 EMBL beamline (DESY) and processed using the HKL-2000 suite of programs.[20] Crystals exhibited the symmetry of space group $P4_3$ and contained 2 molecules in the asymmetric unit. Crystal parameters and data collection statistics are given in supplemental Table 1.

Structure determination

The structure of IRS-2 was solved by molecular replacement using the MoLrep 9.2 program.[21] The search model was derived from the structure of the equine leukocyte elastase inhibitor in R-state conformation (Protein Data Bank [PDB] code 1HLE).[22] Model refinement was carried out using the program REFMAC 5.3[23] from the CCP4 package.[24] Manual building was done using Coot.[25] Tight noncrystallographic symmetry restraints were applied during initial refinement; in later stages, the restraints were loosened as guided by the behavior of R_{free}. The final steps included translation, libration, and screw refinement.[26] The quality of the final models was validated with MoLProbity server.[27] Final refinement statistics are given in supplemental Table 1. Figures showing structural representations were prepared with the program PyMOL 0.99 (DeLano Scientific).[28] The DALI server was used to search for structural homologs.[29] Ramachandran plot statistics were determined by PROCHECK.[30]

Results

Cloning of serpins from *I ricinus*

The sequences of numerous serine protease inhibitors from the serpin superfamily have been identified from various ixodid tick

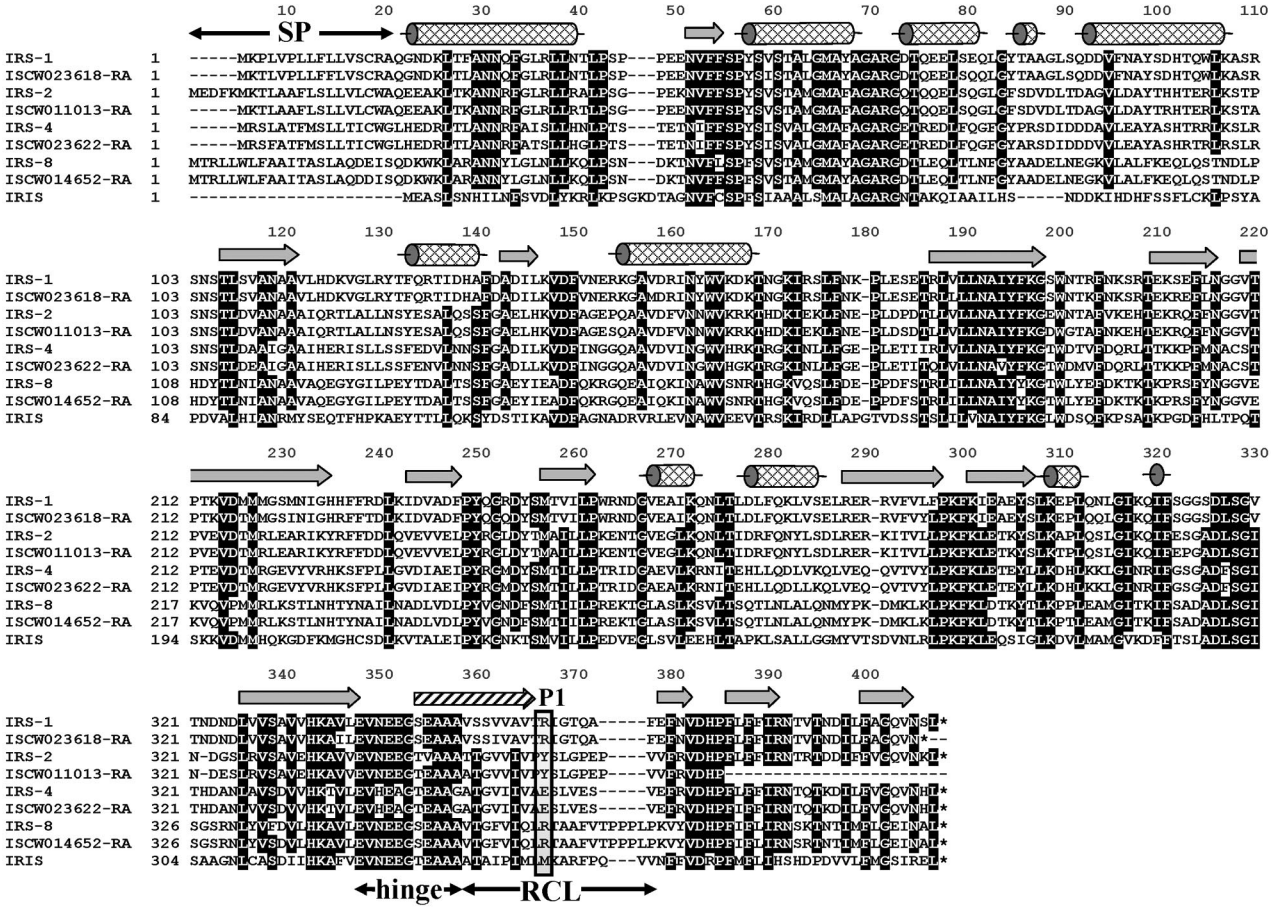

Figure 1. Alignment of the 4 full-length *I ricinus* serpin clones with their orthologs from *I scapularis* obtained from the completed *I scapularis* genome. All serpins are compared with IRIS, the only functionally characterized tick serpin so far. Unlike IRIS, IRS-2 has a clear signal peptide (residues 1-21). The secondary structure elements are indicated according to the IRS-2 crystal structure: α-helixes (cylinders), β-strands (arrows); the hatched arrow represents the region that undergoes a conformational change from a loop to a β-strand after proteolytic cleavage of RCL. SP, signal peptide; hinge, hinge region, an important determinant of serpin inhibitory potential; RCL, reactive center loop; P1 (rectangle), predicted residue behind which the target protease cleaves the RCL.

species, and it is also known that the family is represented in *I ricinus* salivary glands.[14] However, the knowledge of *I ricinus* salivary serpins, and the function of tick serpins in general, is limited to IRIS, a serpin that does not follow a classical secretion pathway from the salivary glands. Therefore, with the aim to identify classically secreted *I ricinus* serpins (ie, those containing a clear signal peptide), we designed degenerate primers based on the 2 most conserved domains (NAIYFKG and PFLFFI) found in the alignment of 10 arthropod serpins, for which sequence data were available at that time. The obtained PCR-amplified fragment was radioactively labeled and used for the screening of a cDNA library prepared from salivary glands isolated from adult female ticks after 5 days of attachment to the host to find as many serpin clones as possible. Four different full-length serpin cDNA clones that contained signal peptide, namely, IRS-1, -2, -4, and -8 (National Center for Biotechnology Information accession numbers DQ915842, DQ915843, DQ915844, and DQ915845), were identified. Orthologs for all 4 genes can be found in the genome of *I scapularis* (http://iscapularis.vectorbase.org/index.php), the vector of Lyme disease pathogens in the Eastern and Central parts of the United States. Amino-acid identity between the corresponding serpin orthologs varies from 94.9% for IRS-4 to 98.8% for IRS-8. The alignment in Figure 1 compares the 4 discovered serpins with the homologous proteins from *I scapularis* and with IRIS.[14] All proteins, including IRIS, display putative inhibitory features in the serpin hinge region, and all proteins except IRIS bear a clear signal peptide, suggesting a classical secretory mechanism from the salivary glands. Based on their amino acid (aa) sequence and on the preliminary prediction of the P1 position of each serpin, we proceeded with further analysis of IRS-2. More specifically, the predicted P2-P2′ sequence of the IRS-2–reactive center loop is Pro-Tyr-Ser-Leu with the tyrosine at the P1 position, suggesting antichymotrypsin, rather than antitrypsin, specificity. Mature IRS-2 is a 376-aa protein, weakly acidic with pI 5.53; the predicted molecular weight was 41.9 kDa. The unprocessed protein contains a 21-aa predicted signal peptide, according to the SignalP 3.0 server program.

IRS-2 expression is up-regulated after tick attachment

Next, we determined the expression profile of IRS-2 in different tick tissues throughout the feeding period of adult ticks using quantitative real-time PCR (Figure 2). IRS-2 displayed 36 times higher mRNA expression in tick salivary glands at day 6 after tick attachment to the host, compared with salivary glands derived from unfed ticks. Already, at day 2 after attachment, the expression was 9-fold higher than in unfed ticks, suggesting a role in the tick salivary glands, even in the early stage of tick feeding. The increase of IRS-2 gene expression was also notable in tick ovaries, with a 4-fold increase at day 6 after attachment. Finally, IRS-2 transcript abundance fluctuated in the tick midgut as feeding progressed.

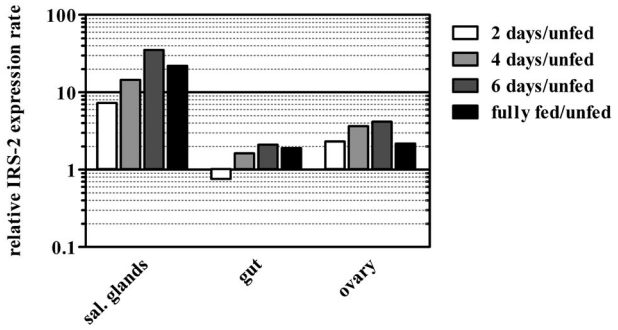

Figure 2. Expression of IRS-2 is up-regulated after tick attachment to the host. IRS-2 transcripts accumulate rapidly in salivary glands after the attachment of an adult *I ricinus* female, less rapidly in its ovaries, and they remain almost unchanged in its midgut. Each bar in the graph represents the ratio between IRS-2 transcript abundance in a certain tick tissue and a given tick feeding stage, compared with the corresponding tissue from unfed ticks (ie, the black bar in the salivary glands part of the graph shows that the transcript abundance of IRS-2 mRNA is 20× higher in the salivary glands of fully fed adult female ticks than in the salivary glands of unfed females). The scale in the y-axis is logarithmic.

IRS-2 inhibits acute inflammation

Induction of IRS-2 transcription in the salivary glands upon blood feeding and the known anti-inflammatory properties of tick saliva led us to investigate whether IRS-2 could contribute to the immunomodulatory activity of tick saliva. For this purpose, we produced recombinant IRS-2 in a bacterial expression system and proceeded with lipopolysaccharide decontamination. Subsequently, we assessed its effect in a mouse model of acute inflammation. It is well described that when carrageenan is inoculated in the mouse footpad, it induces an acute inflammatory response characterized by edema formation in the paw accompanied by neutrophil influx.[31] To investigate whether IRS-2 could modulate carrageenan-induced inflammation, carrageenan was administered in the mouse footpads in the presence or absence of IRS-2. When carrageenan was injected in the presence of IRS-2, a dose-dependent inhibition of edema formation was observed (Figure 3 A). More specifically, in the presence of 1 mg/kg of IRS-2, the thickness of the mouse paw was similar to that of negative controls; that is, PBS-injected mice (data not shown) or mice injected with IRS-2 only (Figure 3A). The decrease in edema formation reached 67.2% ($P < .001$) at 4 hours after injection, compared with positive control (carrageenan-injected footpads). This was not 100% because there was a background increase in paw thickness even when injecting vehicle alone, since the inoculum (40 μL of liquid) could not be completely absorbed by the footpad within 4 hours. The inhibition observed after 4 hours of carrageenan injection with IRS-2 at the concentration 0.3 mg/kg was 23.4%, compared with positive control, and it was not statistically significant (Figure 3A). At 24 hours after injection, there were no differences in edema formation in any of the experimental groups of mice. Next, we analyzed carrageenan-induced recruitment of neutrophils in the footpads by measuring tissue MPO activity. The experimental design was the same as in the paw edema experiment. MPO activity in the tissue was evaluated at 4 hours after injection, the time point at which edema peaks. Statistically significant inhibition ($P < .05$) of MPO activity (34.3%) was observed even when 0.3 mg/kg of IRS-2 was coadministered with carrageenan. Inhibition reached 71.6% when 1 mg/kg of IRS-2 was coadministered with carrageenan ($P < .001$; Figure 3B). Finally, we normalized the detected MPO activity for the number of neutrophils per milligram of inflamed tissue, and we further evaluated the effect of chymostatin (a generic inhibitor of

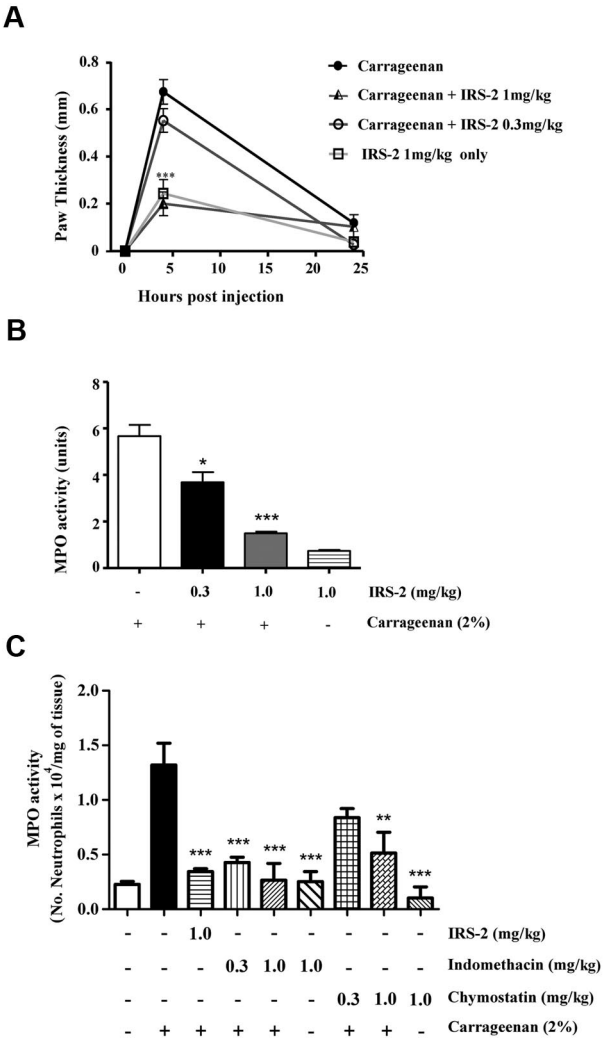

Figure 3. IRS-2 inhibits carrageenan-induced acute inflammation. Mice received carrageenan injections intraplantary in either the absence or presence of 0.3 or 1 mg/kg IRS-2. (A) Edema formation was evaluated at 4 and 24 hours after injection (abscissa) as the increase in paw thickness (in millimeters). (B) Neutrophil recruitment in inflamed footpads was evaluated by measuring tissue myeloperoxidase activity, expressed as units of activity/g of tissue (ordinate). Bar 1 (numbering left to right), activity detected when only carrageenan was administered to mice; bars 2 and 3, effect of coadministration of carrageenan with 0.3 and 1 mg of IRS-2 per 1 kg of body weight, respectively. Bar 4, IRS-2 injected without carrageenan. (C) Mice received injections of saline (-), carrageenan, carrageenan plus IRS-2 (1 mg/kg), indomethacin (0.3 and 1 mg/kg) or chymostatin (0.3 and 1 mg/kg). At 4 hours after injection, the hind paws were collected for MPO analysis and the amount of neutrophils per milligram of tissue was estimated by comparison with purified neutrophils. Asterisks represent statistically significant differences in MPO activity (*$P < .05$; **$P < .01$; and ***$P < .001$), compared with groups injected with carrageenan only (1-way analysis of variance followed by Tukey post-hoc test; n:4 in each group).

primarily chymotrypsin-like serine proteases) and indomethacin (a nonsteroidal anti-inflammatory compound) on MPO activity/neutrophil migration. Both effectors displayed similar inhibitory effect with IRS-2 on neutrophil migration (Figure 3C).

IRS-2 specifically targets cathepsin G and chymase

Given the observed anti-inflammatory effect of IRS-2, we proceeded to a more detailed analysis of the IRS-2 mechanism of action. Considering that serpins are potential inhibitors of serine proteases that play a role in inflammation, and that the bioinformatic analysis of IRS-2 reactive center loop (RCL) suggests an

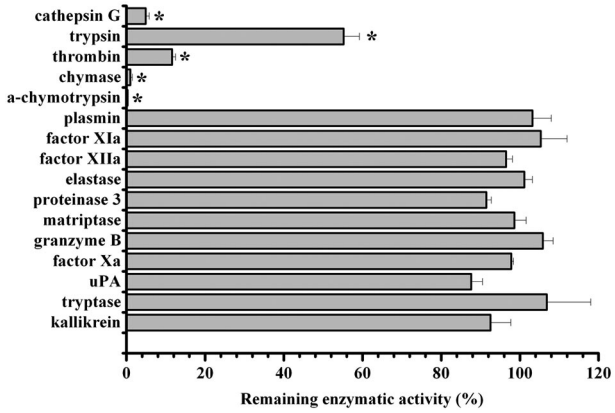

Figure 4. Inhibitory specificity of IRS-2. IRS-2 (400nM) was tested against 16 different serine proteases in triplicates. The enzyme concentration is stated in supplemental Table 2. Bars represent the mean remaining enzymatic activity in the presence of IRS-2, while error bars represent the SEM. Enzymes with an asterisk were inhibited with a statistical significance (*t* test; $P < .05$).

inhibitory specificity against chymotrypsin-like, rather than trypsin-like, serine proteases, we tested the protein for inhibitory activity against a panel of pure recombinant human serine proteases. Recombinant IRS-2 was tested against an array of 14 different physiologically relevant serine proteases, in addition to α-chymotrypsin and trypsin, the 2 archetypes for chymotrypsin- and trypsin-like serine proteases. As shown in Figure 4, IRS-2 inhibited 2 trypsin-like (trypsin and thrombin) and 3 chymotrypsin-like (α-chymotrypsin, cathepsin G, and mast cell chymase) proteases significantly ($P < .05$), with higher activity against the latter group. IRS-2 did not inhibit a series of serine proteases related with the coagulation or inflammation, such as plasmin, factor Xa, factor XIa, or elastase and proteinase 3, suggesting a stringent specificity (Figure 4). Table 1 and Figure 5A-B summarize the concentration-dependence of IRS-2 inhibition for all 5 targeted enzymes. Table 1 further describes the binding characteristics for thrombin, cathepsin G, and chymase, 3 physiologically relevant proteases. For further details on the related biochemical analysis, please see supplemental Results and supplemental Figures 1 and 2.

IRS-2 inhibits mMCP-4

Having dissected the target specificity of IRS-2, and considering that chymase (1 of the 2 targets of IRS-2) is released from mast cells upon acute inflammation, we next investigated whether IRS-2 would bind to mouse (the animal model used for the anti-inflammatory experiments) mast cell protease-4 (mMCP-4). Furthermore, mMCP-4 is the main chymotrypsin-like serine protease produced by connective tissue–type mouse mast cells and is a functional homolog to the human chymase.[32] Therefore, we evaluated the effect of IRS-2 on mMCP-4. Indeed, IRS-2 was found to inhibit mMCP-4 both in vitro and ex vivo. Analogous to the inhibition observed for human chymase, purified mMCP-4 was inhibited by IRS-2 in equimolar concentrations. The estimated inhibitory concentration at half-maximum of IRS-2 against purified mMCP-4 was 5.21nM, when using a 5nM concentration of the enzyme (Figure 5C). Moreover, IRS-2 inhibited the chymotryptic activity present in the suspension of ionomycin-activated PCMCs in a dose-dependent manner (Figure 5C). We also detected the formation of covalent mMCP-4/IRS-2 complexes by Western blot. Notably, mMCP-4/IRS-2 complexes were only detected in association with the cell layer, while no complexes were detected in the conditioned medium. The number of produced complexes was dependent on the concentration of IRS-2 (Figure 5D). More specifically, at 20nM concentration of IRS-2, most of the mMCP-4 remained in the free state, while at 50 and 200nM IRS-2, higher amounts of mMCP-4 were recovered in complex with IRS-2.

IRS-2 inhibits cathepsin G– and thrombin-induced platelet aggregation

Cathepsin G, the second target of IRS-2, plays a role in platelet aggregation, which is crucial in wound-healing processes that are essential for host ability to reject a blood-feeding tick. Therefore, we evaluated the effects of IRS-2 on cathepsin G–induced platelet aggregation, which is mediated by protease-activated receptor 4 (PAR4).[33] Figure 6A shows that cathepsin G–induced shape change and platelet aggregation was completely inhibited by 15-minute incubation with IRS-2 (Figure 6A). In higher excess to the enzyme, IRS-2 inhibited also thrombin-induced platelet aggregation (Figure 6B), which is mediated by PAR1 and PAR4. Collagen-induced (Figure 6C), convulxin-induced[34] (Figure 6D), U46619-induced (Figure 6E), and arachidonic acid-induced (Figure 6F) platelet aggregation remained unaffected, demonstrating the specificity in IRS-2–driven inhibition of platelet aggregation. These results suggest that IRS-2 interferes with platelet aggregation by blocking their activation through PARs, thus implicating IRS-2 as an inhibitor of wound-healing processes.

Structural analysis of IRS-2

Finally, we resolved the crystal structure of IRS-2, which was determined by molecular replacement and refined using data to 1.8 Å resolution. The structure of equine leukocyte elastase inhibitor (PDB code 1HLE) was used as a search model; this homolog had the highest sequence similarity with IRS-2 (35% identity) among the serpin structures available in the PDB. The tetragonal crystal form of IRS-2 contains 2 molecules in the asymmetric unit with solvent content of 45%. The root mean square deviation (RMSD) for superposition of the main-chain atoms of these

Table 1. A tabular representation of IRS-2 inhibition characteristics for the targeted serine proteases

Enzyme	Amount of enzyme used, nM	IRS2 IC_{50}, nM	IC_{50}/enzyme ratio	Inhibitor characteristics
Cathepsin G	12.2	11.5 ± 0.7	0.94	Fast binding tight
Chymase	3.6	4 ± 0.2	1.11	Slow binding tight
Thrombin	0.02	170.3 ± 11	8515	Slow binding classical
α-chymotrypsin	0.038	0.38 ± 0.02	10	N/A
Trypsin	0.25	562.7 ± 27.3	2251	N/A

The amount of enzyme used in the assays as well as the inhibitory concentration at half-maximum (IC_{50}) of IRS-2 for these enzymes is stated in the first and second columns. The third column represents the ratio between IRS-2 IC_{50} and enzyme concentration, and the last column shows the binding characteristics of the inhibitor to the targeted enzymes with the relevance in host physiology (ie, tight or classical inhibitor, fast binding, or slow binding to the enzyme). Because trypsin and α-chymotrypsin were not physiologically relevant to our studies, we did not further study their inhibition characteristics, as depicted in by N/A.

NA indicates not applicable.

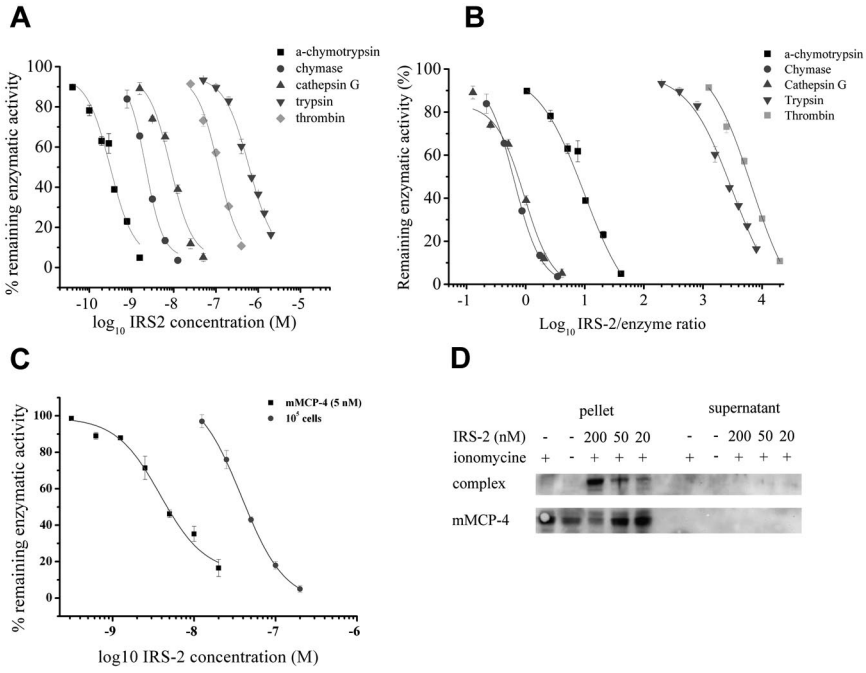

Figure 5. IRS-2 is a serpin with activity against chymotrypsin-like, rather than trypsin-like, serine proteases. (A) Proteases targeted by IRS-2. α-chymotrypsin, chymase, cathepsin G, trypsin, and thrombin are inhibited by IRS-2. The amount of enzyme used is stated in Table 1. The mean remaining enzymatic activity in the presence of various concentrations of IRS-2 is represented, while the error bars represent the SEM in triplicate assays. (B) Inhibition data are normalized by plotting the remaining enzymatic activity (y-axis) against the IRS-2/enzyme ratio (x-axis). (C) Inhibition of purified mMCP-4 (5nM) or present in the suspension of activated mouse PCMCs by IRS-2. The mean remaining enzymatic activity in the presence of various concentrations of IRS-2 is presented (± SEM). (D) Western blot analysis showing covalent complex formation between IRS-2 and mMCP-4 produced by PCMCs. Notably, enzymatic activity and complexes between mMCP-4 and IRS-2 were predominantly cell associated, rather than being present in cell-free supernatants. Cells activated by ionomycin were used as positive control (+), and untreated cells were used as negative control (−). All samples with IRS-2 were activated by ionomycin.

2 molecules is 0.69 Å, a value within the range observed for different crystal structures of identical proteins.[35] Minor structural changes are localized in solvent-exposed loop regions. The N-terminal residue, Met1, represents a cloning artifact that is not part of the native protein sequence. Atomic coordinates of IRS-2 and experimental structure factors have been deposited in the PDB, with the accession code 3NDA.

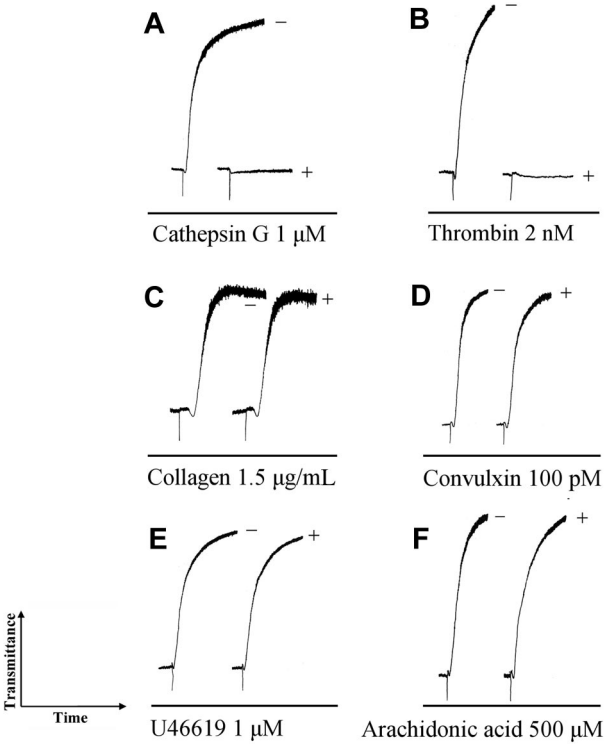

Figure 6. IRS-2 inhibits platelet aggregation induced by cathepsin G. In all experiments, 1.5μM IRS-2 was incubated with the indicated amount of platelet aggregation activator for 15 minutes and the mixture was added to platelets. (−) activator only, (+) activator plus IRS-2.

Figure 7 shows the overall structure of IRS-2. It adopts a typical serpin fold composed of 3 large β-sheets and 9 α-helices. Both molecules in the asymmetric unit adopt a conformation known as the relaxed or R state of the serpins, in which the RCL is cleaved and inserted into the central β-sheet A as a strand, S4 (Figure 7A). Cleavage of RCL occurs during the crystallization process and is catalyzed by traces of contaminating proteases, as demonstrated in the crystallization study.[19] The cleavage site is positioned at residue Tyr341, which represents the P1 substrate residue. In our structure, this residue has a well-defined electron density for its C-terminal carboxyl group. The P1′–P5′ residues of the cleaved RCL are disordered to various extents in the crystal structure; more specifically, residues 342-344 and 342-346 in molecules A and B, respectively, could not be modeled and are missing in the final structure.

A structural comparison of IRS-2 with structures from the serpin superfamily deposited in the PDB identified bovine antithrombin III (PDB code 1ATT) as the closest structural homolog (RMSD approximately 1.4 Å for 369 aligned residues). A lower structural similarity was found to typical representatives of the mammalian serpins, human α-1-antichymotrypsin (PDB code 2ACH, RMSD approximately 1.6 Å for 337 residues), human α-1-antitrypsin (PDB code 9API; RMSD approximately 1.8 Å for 335 residues), and to human corticosteroid-binding globulin and human plasminogen activator inhibitor-1 (PDB codes 2VDX and 3CVM; both RMSD approximately 1.7 Å for 363 residues). All the compared structures are in the R-state conformation; a superposition of selected structures with IRS-2 is presented in Figure 7B.

Discussion

Many *I scapularis* serpins possess Arg at the P1 position,[10] which corresponds to typical cleavage sites for trypsin-like enzymes. This suggests their involvement in modulation or regulation of trypsin-like proteases involved in host-blood coagulation or tick hemolymph, probably with some redundancy in their function. On the

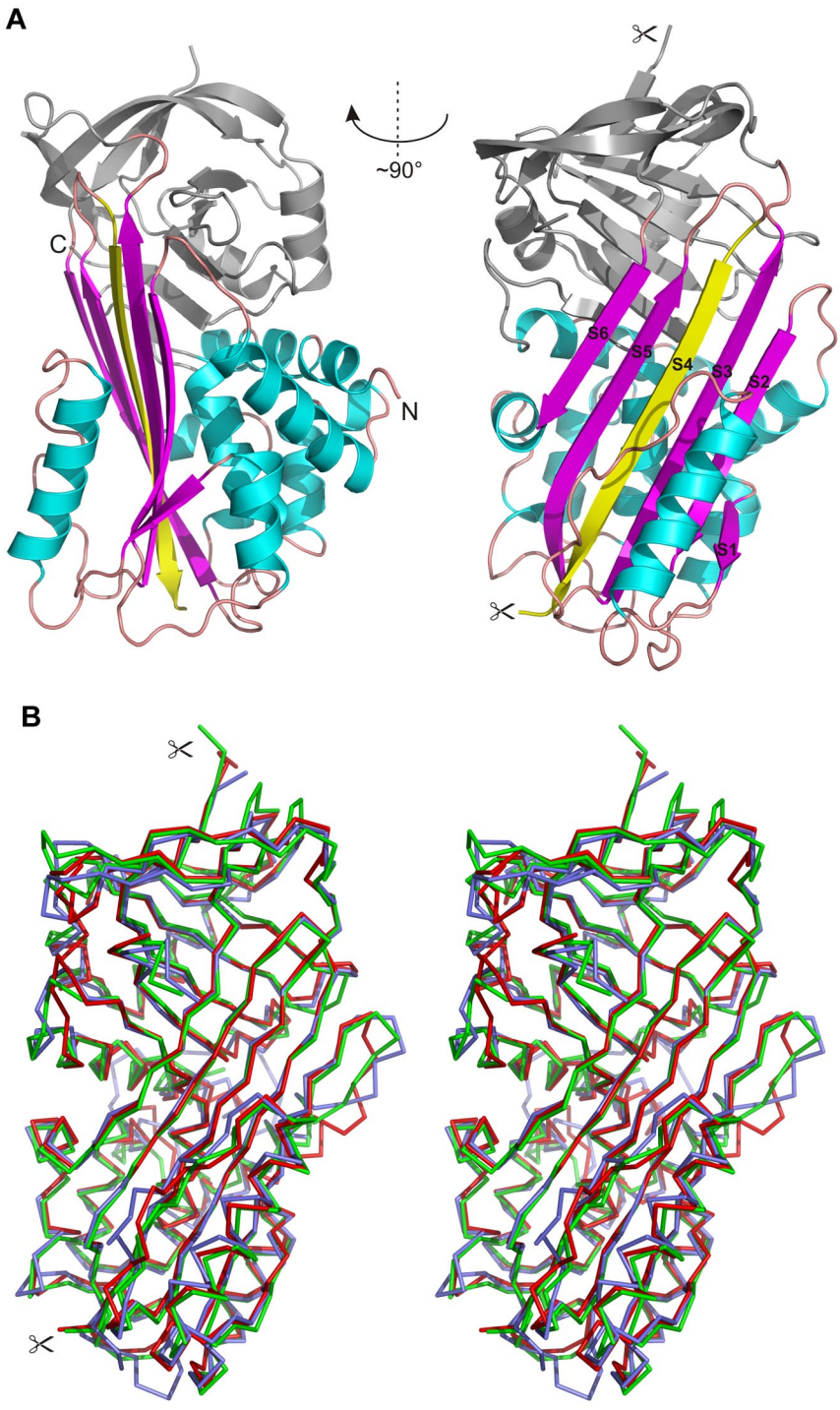

Figure 7. Crystal structure of IRS-2. (A) Overall 3-dimensional structure of IRS-2 in a cartoon representation. The central β-sheet A (magenta) and surrounding helices (cyan) are highlighted. The reactive center loop is cleaved in the relaxed (R-state) conformation of IRS-2 and forms the S4 β-strand (yellow) inserted into the β-sheet A; the termini generated by this proteolytic cleavage are marked by scissors. N- and C-termini of IRS-2 are labeled (N, C). (B) Stereo image showing a superposition of Cα traces of IRS-2 (red) with 2 homologous mammalian serpins in the R-state conformation. Antithrombin III (blue; 1ATT) and α-1-antichymotrypsin (green; 2ACH) display a high level of similarity to IRS-2 with regard to structural homology and inhibitory specificity, respectively.

other hand, only 2 putative serpins that possess the aromatic aa (ie, Trp, Tyr, or Phe) at the P1 position can be found in the *I scapularis* genome, thus having the potential to inhibit chymase and other chymotrypsin-like proteases.[36] According to the nomenclature used by the VectorBase server (http://iscapularis.vectorbase.org), these serpins are encoded by the transcripts, ISCW004156-RA and ISCW011013-RA. The latter transcript is the homolog of IRS-2. Considering the preferential aa residues in the cleavage site for cathepsin G,[37] we believe that IRS-2 is the only known salivary serpin from *I ricinus* that can target both cathepsin G and chymase.

IRS-2 interacts with proteases via a classical "suicide inhibition" mechanism of serpins. It involves cleavage of RCL and formation of S4 β-strand that is inserted in the middle of β-sheet A (Figure 7A). We determined a high-resolution crystal structure of the protease-cleaved IRS-2 that provided an experimental evidence of the Tyr residue at the P1 position. These structural data will be valuable for designing smaller peptides that may mimic IRS-2 inhibitory activities and its pharmacological actions. IRS-2 targets specifically the chymotrypsin-like proteases, cathepsin G and chymase. Both of these proteases are secreted after neutrophil

(cathepsin G) and mast cell (chymase) activation, and they are involved in a whole range of physiological processes associated with the development of an acute inflammatory response and, in particular, in the cross-talk between neutrophils and platelets in the hemostatic process.[38] Cathepsin G is produced mainly by neutrophils, where it is stored in azurophile granules, but it may also be produced in low amounts by mast cells. Cathepsin G is known primarily for its ability to kill engulfed pathogens and for its role in tissue remodeling during inflammation. Furthermore, it is involved in the proteolytic activation of various chemoattractants and hormones as well as in cell signaling by cleaving PAR4, the latter having been identified as an important signaling receptor in inflammation and platelet activation.[39] Cleavage of PAR4 by cathepsin G is responsible for the platelet activation that leads to their aggregation and clot formation. Here, we showed, for the first time, that a tick salivary protein inhibits cathepsin G–induced platelet aggregation, which apparently helps the tick in obtaining its blood meal. In addition, we revealed that in higher molar excess, IRS-2 affects thrombin-induced platelet aggregation as well, further disclosing its multipotential role in inflammation and hemostasis through the modulation of PAR activation.

Besides preventing blood loss after an injury, activated platelets produce several chemokines and their precursors, which are further proteolyticaly processed. In this respect, the role of cathepsin G overlaps with that of chymase. Chymase is produced almost exclusively by mast cells that are resident in mucosal and connective tissues and it processes many substrates, such as angiotensin I, extracellular matrix components, and also several proinflammatory substances, such as interleukin-1β and interleukin-18 precursors.[32] Both cathepsin G and chymase activate connective tissue–activating peptide-III (CTAP-III), which is secreted by activated platelets, into an active neutrophil-activating peptide-2 (NAP-2), the chemokine responsible for further activation of neutrophils and their attraction to the site of injury. It was also shown that chymase is mainly responsible for CTAP-III/NAP-2 conversion, and that activated mast cells displayed a 1000-fold higher conversion rate than activated neutrophils.[40] Other natural substrates for both enzymes are the big endothelins (ETs), the precursors for several vasoconstrictors with different potency. Their cleavage products are 31-aa fragments, denoted Ets (1-31), that, apart from being among the most potent vasoconstrictors, also act as chemoattractants for neutrophils and monocytes.[41] Interestingly, the RCL of IRS-2 strongly resembles the chymase cleavage site in big ETs. The sequence in the P3–P3′ region consists of VPY–SLG for IRS-2 and VPY–GLG for big ETs. We can therefore hypothesize that this is the result of convergent evolution that created almost identical recognition sites that target both cathepsin G and chymase on otherwise unrelated proteins. To our knowledge, this is the first time that a parasitic protein is shown to inhibit host proteases by mimicking host endogenous substrates. Moreover, structural comparison revealed significant structural homology of IRS-2 with α-1-antichymotrypsin, which is supposed to be a natural vertebrate host regulator of cathepsin G and mast cell chymase.

Neutrophil-derived cathepsin G and, in particular, mast cell chymase are present at the early stages of an acute inflammatory response, probably with some level of redundancy and/or cooperation in their functions. By inhibiting both enzymes, IRS-2 can significantly alter a defensive response to tissue destruction caused by a tick bite. Indeed, we demonstrated that IRS-2 inhibits carrageenan-induced acute inflammation and cathepsin G and thrombin-induced platelet aggregation. According to recent findings relating to the biologic function of cathepsin G and mast cell chymase, we can hypothesize that both described effects may be mediated by proteolyticaly activated transducers and receptors during the early steps of inflammatory response that occurs after a tick bite. To explain the observed effects of IRS-2, we suggest that IRS-2 targets neutrophils, platelets, and mast cells at the early steps of their activation by preventing cathepsin G– or thrombin-driven platelet activation, which may lead to reduced CTAP-III release. Subsequently, IRS-2, similar to chymase inhibitors,[40] inhibits the cathepsin G– and chymase-catalyzed conversion of CTAP-III into NAP-2, resulting in impaired extravasation of neutrophils. The direct proof of the suggested, literature-based hypothesis exceeds the purpose of this work.

Here, we describe a mechanism of vertebrate host modulation that is novel not only for a tick salivary component, but to our knowledge for any parasite. Moreover, the dual specificity of IRS-2 for both cathepsin G and chymase is rare even among natural serine protease inhibitors in general. The saliva of *I ricinus* is a complex mixture of many proteins, including protease inhibitors with unknown specificity and function. This work describes a novel salivary protein that is unique among other salivary serpins of *Ixodes spp*—and proteases inhibitors in general—regarding both specificity and the mode of action in the vertebrate host. Therefore, the herein described findings contribute to our understanding of vertebrate physiology and parasite-host interaction, while the herein disclosed structural basis of IRS-2 activity can lead to the development of pharmaceutical applications in the near future.

Acknowledgments

We thank Ida Waern and Elin Rönnberg from the Swedish University of Agricultural Sciences for help with mast cell experiments and the Swedish Research Council for financial support. We also thank Jan Erhart (Institute of Parasitology, Biology Center of the Academy of Sciences of Czech Republic) for providing ticks; Anderson Sá-Nunes (Institute of Biomedical Sciences, University of São Paulo) for discussions and help with the experimental design; and NIAID intramural editor Brenda Rae Marshall for assistance. We also thank the anonymous reviewers for critical and constructive comments and the editorial team of *Blood* for efficiently processing the manuscript.

This work was supported by grant no. IAA600960811 from the Grant Agency of the Academy of Sciences of the Czech Republic, Research Center no. LC06009 from the Ministry of Education, Youth and Sports of the Czech Republic, and by grant no. Z60220518 of the Academy of Sciences of the Czech Republic. The structural element was supported by grant no. P207/10/2183 from the Grant Agency of the Czech Republic and research project Z40550506. Diffraction data were collected at beam line X12, EMBL-Hamburg outstation at DESY (Hamburg, Germany). I.M.B.F., J.M.C.R., and M.K. were supported by the Intramural Research Program of the Division of Intramural Research, National Institute of Allergy and Infectious Diseases, NIH, and M.K. by a Jan Evengelista Purkyne fellowship of the Academy of Sciences of the Czech Republic.

Because I.M.B.F. and J.M.C.R. are government employees and this is a government work, the work is in the public domain in the United States. Notwithstanding any other agreements, the NIH reserves the right to provide the work to PubMedCentral for display and use by the public, and PubMedCentral may tag or modify the work consistent with its customary practices. One can establish

Authorship

Contribution: J.C., C.J.O., I.M.B.F., M.M., and M.K. designed and performed experiments, analyzed data, and wrote the manuscript; P.R. and Z.K. designed and performed experiments; and G.P., P.K., J.M.C.R., and J.K. designed experiments and analyzed data.

Conflict-of-interest disclosure: The authors declare no competing financial interests.

Correspondence: Michail Kotsyfakis, Institute of Parasitology, Biology Center of the Academy of Sciences of Czech Republic, Branisovska 31, 37005 Ceske Budejovice, Czech Republic; e-mail: kotsyfakis@paru.cas.cz.

References

1. Ribeiro JM, Makoul GT, Levine J, Robinson DR, Spielman A. Antihemostatic, anti-inflammatory, and immunosuppressive properties of the saliva of a tick, Ixodes dammini. *J Exp Med.* 1985;161(2): 332-344.
2. Francischetti IM, Sa-Nunes A, Mans BJ, Santos IM, Ribeiro JM. The role of saliva in tick feeding. *Front Biosci.* 2009;14:2051-2088.
3. Deruaz M, Frauenschuh A, Alessandri AL, et al. Ticks produce highly selective chemokine binding proteins with anti-inflammatory activity. *J Exp Med.* 2008;205(9):2019-2031.
4. Kotsyfakis M, Sa-Nunes A, Francischetti IM, Mather TN, Andersen JF, Ribeiro JM. Antiinflammatory and immunosuppressive activity of sialostatin L, a salivary cystatin from the tick, Ixodes scapularis. *J Biol Chem.* 2006;281(36): 26298-26307.
5. Ribeiro JM, Alarcon-Chaidez F, Francischetti IM, et al. An annotated catalog of salivary gland transcripts from Ixodes scapularis ticks. *Insect Biochem Mol Biol.* 2006;36(2):111-129.
6. Chmelar J, Anderson JM, Mu J, Jochim RC, Valenzuela JG, Kopecky J. Insight into the sialome of the castor bean tick, Ixodes ricinus. *BMC Genomics.* 2008;9:233.
7. Francischetti IM, My Pham V, Mans BJ, et al. The transcriptome of the salivary glands of the female western black-legged tick, Ixodes pacificus (Acari: Ixodidae). *Insect Biochem Mol Biol.* 2005; 35(10):1142-1161.
8. Potempa J, Korzus E, Travis J. The serpin superfamily of proteinase inhibitors: structure, function, and regulation. *J Biol Chem.* 1994;269(23): 15957-15960.
9. Irving JA, Pike RN, Lesk AM, Whisstock JC. Phylogeny of the serpin superfamily: implications of patterns of amino acid conservation for structure and function. *Genome Res.* 2000; 10(12):1845-1864.
10. Mulenga A, Khumthong R, Chalaire KC. Ixodes scapularis tick serine proteinase inhibitor (serpin) gene family: annotation and transcriptional analysis. *BMC Genomics.* 2009;10:217.
11. Mulenga A, Khumthong R, Blandon MA. Molecular and expression analysis of a family of the Amblyomma americanum tick, Lospins. *J Exp Biol.* 2007;219(18):3188-3198.
12. Sugino M, Imamura S, Mulenga A, et al. A serine proteinase inhibitor (serpin) from ixodid tick, Haemaphysalis longicornis: cloning and preliminary assessment of its suitability as a candidate for a tick vaccine. *Vaccine.* 2003;21(21-22): 2844-2851.
13. Mulenga A, Tsuda A, Onuma M, Sugimoto C. Four serine proteinase inhibitors (serpin) from the brown ear tick, Rhiphicephalus appendiculatus: cDNA cloning and preliminary characterization. *Insect Biochem Mol Biol.* 2003;33(2):267-276.
14. Leboulle G, Crippa M, Decrem Y, et al. Characterization of a novel salivary immunosuppressive protein from Ixodes ricinus ticks. *J Biol Chem.* 2002;277(12):10083-10089.
15. Prevot PP, Adam B, Boudjeltia KZ, et al. Antihemostatic effects of a serpin from the saliva of the tick, Ixodes ricinus. *J Biol Chem.* 2006; 281(36):26361-26369.
16. Prevot PP, Beschin A, Lins L, et al. Exosites mediate the anti-inflammatory effects of a multifunctional serpin from the saliva of the tick, Ixodes ricinus. *FEBS J.* 2009;276(12):3235-3246.
17. Sambrook J, Fritsch EF, Maniatis T. *Molecular Cloning: A Laboratory Manual.* 2nd ed. Cold Spring Harbor, NY: Cold Spring Harbor Press; 1989.
18. Andersen JF, Francischetti IM, Valenzuela JG, Schuck P, Ribeiro JM. Inhibition of hemostasis by a high affinity biogenic amine-binding protein from the saliva of a blood-feeding insect. *J Biol Chem.* 2003;278(7):4611-4617.
19. Kovářová Z, Chmelař J, Šanda M, Brynda J, Mareš M, Řezáčová P. Crystallization and diffraction analysis of the serpin, IRS-2, from the hard tick, *Ixodes ricinus. Acta Crystallogr F Struct Biol Cryst Commun.* In press.
20. Minor W, Cymborowski M, Otwinowski Z, Chruszcz M. HKL-3000: the integration of data reduction and structure solution—from diffraction images to an initial model in minutes. *Acta Crystallogr D Biol Crystallogr.* 2006;62(8):859-866.
21. Vagin A, Teplyakov A. An approach to multi-copy search in molecular replacement. *Acta Crystallogr D Biol Crystallogr.* 2000;56(12):1622-1624.
22. Baumann U, Bode W, Huber R, Travis J, Potempa J. Crystal structure of cleaved equine leucocyte elastase inhibitor determined at 1.95 A resolution. *J Mol Biol.* 1992;226(4):1207-1218.
23. Murshudov GN, Vagin AA, Dodson EJ. Refinement of macromolecular structures by the maximum-likelihood method. *Acta Crystallogr D Biol Crystallogr.* 1997;53(3):240-255.
24. CCP4. The CCP4 suite: programs for protein crystallography. *Acta Crystallogr D Biol Crystallogr.* 1994;50(5):760-763.
25. Emsley P, Cowtan K. Coot: model-building tools for molecular graphics. *Acta Crystallogr D Biol Crystallogr.* 2004;60(12,1):2126-2132.
26. Winn MD, Isupov MN, Murshudov GN. Use of TLS parameters to model anisotropic displacements in macromolecular refinement. *Acta Crystallogr D Biol Crystallogr.* 2001;57(1):122-133.
27. Davis IW, Leaver-Fay A, Chen VB, et al. MolProbity: all-atom contacts and structure validation for proteins and nucleic acids. *Nucleic Acids Res.* 2007;35(Web Server issue):W375-W383.
28. De Lano WL. *The PyMOL Molecular Graphics System.* San Carlos, CA: DeLano Scientific LLC; 2002.
29. Holm L, Sander C. Searching protein structure databases has come of age. *Proteins.* 1994;19(3):165-173.
30. Laskowski RA, Macarthur MW, Moss DS, Thornton JM. Procheck—a program to check the stereochemical quality of protein structures. *J Appl Cryst.* 1993;26:283-291.
31. Levy L. Carrageenan paw edema in the mouse. *Life Sci.* 1969;8(11):601-606.
32. Pejler G, Abrink M, Ringvall M, Wernersson S. Mast cell proteases. *Adv Immunol.* 2007;95: 167-255.
33. Sambrano GR, Huang W, Faruqi T, Mahrus S, Craik C, Coughlin SR. Cathepsin G activates protease-activated receptor-4 in human platelets. *J Biol Chem.* 2000;275(10):6819-6823.
34. Francischetti IM, Saliou B, Leduc M, et al. Convulxin, a potent platelet-aggregating protein from Crotalus durissus terrificus venom, specifically binds to platelets. *Toxicon.* 1997;35(8):1217-1228.
35. Betts MJ, Sternberg MJ. An analysis of conformational changes on protein-protein association: implications for predictive docking. *Protein Eng.* 1999;12(4):271-283.
36. Andersson MK, Enoksson M, Gallwitz M, Hellman L. The extended substrate specificity of the human mast cell chymase reveals a serine protease with well-defined substrate recognition profile. *Int Immunol.* 2009;21(1):95-104.
37. Rehault S, Brillard-Bourdet M, Juliano MA, Juliano L, Gauthier F, Moreau T. New, sensitive fluorogenic substrates for human cathepsin G based on the sequence of serpin-reactive site loops. *J Biol Chem.* 1999;274(20):13810-13817.
38. Zarbock A, Polanowska-Grabowska RK, Ley K. Platelet-neutrophil-interactions: linking hemostasis and inflammation. *Blood Rev.* 2007;21(2): 99-111.
39. McDougall JJ, Zhang C, Cellars L, Joubert E, Dixon CM, Vergnolle N. Triggering of proteinase-activated receptor 4 leads to joint pain and inflammation in mice. *Arthritis Rheum.* 2009;60(3): 728-737.
40. Schiemann F, Grimm TA, Hoch J, et al. Mast cells and neutrophils proteolytically activate chemokine precursor CTAP-III and are subject to counter-regulation by PF-4 through inhibition of chymase and cathepsin G. *Blood.* 2006;107(6): 2234-2242.
41. Cui P, Tani K, Kitamura H, et al. A novel bioactive 31-amino-acid, endothelin-1, is a potent chemotactic peptide for human neutrophils and monocytes. *J Leukoc Biol.* 2001;70(2): 306-312.